Research Paper

Lipid-Coated Mesoporous Silica Particles for pH-Sensitive Tumor-Targeted Paclitaxel: Development, Characterization

Yingyue Deng[1,2], Tao Zhang[1,2], Jiaru Zhou[1,2], Zhihao Su[1], Yingsong Cao[1], Junxi Luo[1], Leming Zhao[1], Junjie Hua[1], Guoqiang Wang[1], Min Xiao[1], Junfeng Ban[1,2], Yan Zhang[1,2✉] and Hongcai Liang[3✉]

1. Guangdong Pharmaceutical University; Guangzhou, China.
2. The Innovation Team for Integrating Pharmacy with Entrepreneurship, Guangdong Pharmaceutical University, Guangzhou, China.
3. Guangdong Provincial Hospital of Chinese Medicine, The Second Affiliated Hospital of Guangzhou University of Chinese Medicine, Guangdong Provincial Academy of Chinese Medical Sciences, Guangzhou, Guangdong 510006, China.

✉ Corresponding authors: Yan Zhang (Email: yanzhang@gdpu.edu.cn) and Hongcai Liang (Email: lianghongcai@gzucm.edu.cn).

Abstract

Nanoparticle carriers can selectively deliver the drug cargo to tumor cells, thus having the ability to prevent early drug release, reduce non-specific cell binding, and prolong *in vivo* drug retention. We constructed paclitaxel (PTX)-loaded lipid-shell mesoporous silica nanoparticles (LMSNs) for targeted anti-cancer drug delivery. The physical properties of PTX-LMSNs were analyzed by scanning electron microscopy (SEM) and transmission electron microscopy (TEM). The drug loading (*DL%*) and entrapment efficiency (*EE%*) of PTX-LMSNs were measured by high performance liquid chromatography (HPLC). *In vitro* drug release test, *in vivo* imaging, tissue distribution and pharmacokinetics of PTX-LMSNs were also evaluated. The SEM examination showed that MSNs were sphere, whereas TEM showed that they were rich in fine pores. The uniform core-shell structure of PTX-LMSNs was also verified by TEM. The DL capacity of PTX-LMSN was as high as 21.75%, and PTX was released from the nanoparticles *in vitro* in a pH-dependent manner. The cumulative amount of free PTX increased at lower pH, which is conducive to selective drug release from LMSNs in the acidic tumor tissues. *In vivo* imaging showed prolonged retention of PTX-LMSNs, which is beneficial to their therapeutic efficacy. In addition, PTX-LMSNs were primarily concentrated in the liver. Pharmacokinetic experiments showed that the half-life of PTX-LMSNs was 23.21% longer and 79.24% higher than that of Taxol. Together, LMSNs are a highly promising antineoplastic drug carrier system.

Keywords: Paclitaxel; mesoporous silica nanoparticles; liposomes; antitumor; pH sensitivity; controllable drug delivery

Introduction

Chemotherapy is still an indispensable tool for treating advanced cancer. However, the inability of traditional anti-cancer drugs to specifically target tumor cells not only leads to serious systemic side effects but also limits their therapeutic effects. In recent years, nanoparticle drug delivery systems, such as liposomes, polymeric micelles, and multimers, have attracted extensive research attention in the field of antitumor drug carriers due to their unique drug loading capacity, targeted delivery characteristics, and controllable release performance [1-3]. Nanoscale carriers achieve passive tumor targeting by enhancing the osmotic retention effect (EPR), significantly increasing the accumulation concentration of drugs in tumor tissues, and improving the solubility and stability of hydrophobic drugs [4, 5]. However, traditional carriers prepared by nano-preparations such as liposomes are unstable in body fluids and also release the drug cargo before reaching the tumor, resulting in serious adverse effects [6, 7].

Particle size is an important parameter for efficient delivery of nanocarriers to tumor sites, as well as for their high adsorption on the tumor cell surface, cellular uptake and intracellular transport,

which eventually determine the efficacy of chemotherapy [8-10]. Stimuli-responsive drug delivery systems dynamically adjust the particle size in response to changes in pH, enzyme, heat or magnetic field of the tumor microenvironment, prolong the cycle and enhance the EPR effect in the early stage, and promote tumor penetration in the later stage, which can significantly improve the ability to penetrate deep tumor tissues, thereby optimizing the efficiency of drug delivery and balancing the contradiction between permeability and retention [11-13].Therefore, stimuli-responsive drug delivery systems can enhance the targeted accumulation of drugs at the lesion site, thereby improving the therapeutic effect and possibly reducing damage to normal tissues [14-16]. Stimulus-responsive drug delivery systems are designed to respond to a variety of physical and chemical stimuli such as temperature, electric field, pH, magnetic field, and ionic strength, with pH and temperature being widely used because they do not require additional lasers and cause less damage to normal tissues [17].

Mesoporous silica is biodegradable, and the degradation product, silicic acid, can be absorbed and excreted through the urinary system. Lee [18] reported that 0.1 mg/mL mesoporous silica nanoparticles (MSNs) could be completely degraded within 7 days in simulated body fluids *in vitro*. Although mesoporous silica nanoparticles (MSNs) have good biocompatibility, they still have two major limitations in practical applications: first, the drug is easy to leak in advance during delivery, and it is difficult to achieve precise targeted and controlled release; Second, the uptake efficiency is low in some specific cell types, such as primary cells and non-phagocytic cells, which directly affects the delivery and therapeutic efficacy of the drug. These deficiencies limit the wide application of MSN in clinical treatment to a certain extent [19]. Nevertheless, owing to their high surface area, pore volume, uniformity, biocompatibility and biodegradability, MSNs are highly promising inorganic drug carriers [20-22].

Lipid-shell and mesoporous silica core nanoparticles (LMSNs) combine the characteristics of nanoparticles and liposomes. The dual vesicular and particulate structure is associated with high biocompatibility, stability and favorable pharmacokinetic profile [23, 24]. Furthermore, drugs can be efficiently encapsulated within the polymer core or between the lipid bilayers of LMSNs, thus allowing LMSNs to have high loading capacity [25]. The polymer core might also delay drug diffusion and increase the stability of the lipid shell, thereby enhancing the encapsulation efficiency (EE) and

system stability [26]. In contrast, polymer micelles are relatively less stable because they are thermodynamic self-assembled structures formed by reversible stabilizing forces such as hydrophobic effects and electrostatic interactions, which will inevitably be disintegrated by multiple instability mechanisms in complex *in vivo* environments, resulting in drug leakage, protein adsorption, and dilution below critical micelle concentrations [27]. However, it is challenging to achieve high EE and optimal particle size when LMSNs is incorporated into hydrophilic drugs. To this end, we are committed to the development of a high-efficiency paclitaxel (PTX) delivery system based on mesoporous silica nanoparticles (LMSNs), PTX-LMSNs. PTX-LMSNs makes full use of the advantages of high drug loading capacity and small particle size of mesoporous silica nanoparticles, and significantly improves the encapsulation efficiency and tumor targeting of the drug through careful surface modification and stimulus response design, effectively overcoming the defects of traditional polymer micelle drugs that are easy to leak and insufficient targeting, thereby greatly enhancing the anti-tumor effect and treatment accuracy of paclitaxel. LMSNs were prepared using a modified method, and PTX-LMSNs were comprehensively characterized. The distribution of the nanovehicles in mice was observed by real time *in vivo* imaging. The *in vivo* pharmacokinetics of the drug was also evaluated.

Materials and Methods

Materials

Paclitaxel (PTX) was purchased from Hainan Yayuan Pharmaceutical Co. Ltd. (Hainan, China), ethyl orthosilicate (TEOS) was from Aladdin Chemical Reagent Co. Ltd. (Shanghai, China), cetyltrimethyl ammonium bromide (CTAB) was from McLean Chemical Reagent Co. Ltd. (Shanghai, China), $NaHCO_3$ was from Tianjin Zhiyuan Chemical Reagent Factory (Tianjin, China), and 15-hydroxy stearic acid polyethylene glycol (Solutol HS-15) was from BASF Company. Egg yolk lecithin (PL100M) was purchased from Shanghai AVT Pharmaceutical Technology Co. Ltd. (Shanghai, China). Other chemicals and solvents were of analytical grade.

Synthesis of mesoporous silica core-lipid bilayer shell nanoparticles

The preparation of MSNs started by dissolving 1.5 g of CTAB and K_2SO_4 in a 255 ml solution consisting of 5 mL of 95% ethanol and 0.5 M $NaHCO_3$ ammonia (solution 1). Solution 2 was then prepared by mixing 5 mL of 0.5 M $Ca(COO)_2$ in 5 mL of 95%

ethanol. The two solutions were quickly mixed with 10 mL of TEOS and then stirred at 600 r/min at room temperature for 6 h. After aging for 4 h, the reaction products were washed thrice with 75% ethanol at 4000 r/min, purified and then dried in vacuum at 65 °C. The dried mesoporous silica carrier was soaked in 0.1 M hydrochloric acid, washed thrice with 75% ethanol at 4000 r/min, and then dried in vacuum at 65 °C. Subsequently, it was calcined in a muffle furnace at 250 °C for 0.5 h and then heated to 550 °C for 4 h to obtain MSNs.

The description of lipid-modified MSNs is shown in Table 1, and the lipid-modified MSNs were prepared by post-loading method [28, 29]. Briefly, 63 mg of PTX was dissolved in 5 volumes of dichloromethane in a penicillin vial, and 3-fold MSNs were then added. The mixture was stirred at 500 r/min for 4 h in the dark at room temperature. After removing the organic solvents, 50 mL of aqueous solution containing 0.5% Solutol HS-15 was poured into a round-bottomed flask, and lecithin and oleic acid were added thereafter using the membrane dispersion method. The lipids were dissolved in 25 mL of trichloromethane, and the solvent was evaporated at 40 °C until a uniform and transparent lipid film was formed. The MSN preparation was suspended in a hydration solution, and the resultant solution was poured over the lipid coating and then swirled until the lipid membrane was completely dissolved [30]. After that, it was continuously sonicated at 100 W for 5 min using an ultrasonic processor before being filtered through a 0.22 µm nylon microporous membrane. The filtrate was then added with a small volume of ampoule while passing nitrogen, and the obtained PTX-LMSNs were stored at 4 °C.

Table 1. The prescription of lipid modification of mesoporous silica nanoparticles.

Component	Content
Paclitaxel	1.10%
MSN	3.30%
Oleic acid	0.29%
Soybean Phospholipid	2.90%
Solutol HS-15	0.48%
Trichloromethane	q.s.
Dichloromethane	q.s.
Water	Add up to 100%

Characterization of nanoparticles

The morphology of MSNs was observed by scanning electron microscopy (SEM, JSM-7500F, JEOL, Japan) and transmission electron microscopy (TEM, JEM-1400, JEOL, Japan), and the morphology of PTX-LMSNs was observed by TEM. MSNs were gilded before being observed under a scanning electron microscope. The MSNs were dispersed in deionized water to a concentration of 2 mg/mL prior to TEM examination, while the PTX-LMSNs were diluted by 10 times. The particle size and polydispersion index (PDI) of PTX-LMSNs were measured by a Delsa Nano C (Beckman Coulter, USA), and their morphology was observed under a transmission electron microscope. Nitrogen adsorption-desorption was analyzed by a JW-BK 132F specific surface area and porosity analyzer (Beijing, China). The specific surface area was calculated by Brunauere-Emmette-Teller (BET) method, and the cumulative pore volume was calculated by Barrett-Joyner-Halenda (BJH) model.

Drug content and encapsulation efficiency (EE%)

The drug loading (*DL*%) capacity of PTX-LMSNs was measured by high performance liquid chromatography (HPLC, 1260, Agilent Technologies, USA) using a Kromasil C18 (4.6 mm × 250 mm, 5 µm) column. The mobile phase consisted of methanol, acetonitrile and distilled water. The flow rate was 1 mL, the injection volume was 20 µL and the detection wavelength was 229 nm. To extract PTX, 1 mL of PTX-LMSN was mixed with 9 mL of acetonitrile, and the solution was filtered through a 0.22 µm membrane. The filtrate was injected into the HPLC instrument to determine the *DL* of PTX-LMSNs. PTX-LMSNs were extracted and separated by dextran chromatography, followed by HPLC to determine the entrapment efficiency (*EE*%). The SephadexG-50 separation column (1.5 cm × 13 cm) was equilibrated for 12 h before being loaded with 0.5 mL of PTX-LMSNs. The flow rate of the eluant was 3 mL/min, and the eluent was collected every 2 mL. After eluting with 30 mL of distilled water, the appropriate amount of eluent was collected and then mixed with 3 mL of acetonitrile to determine the amount of encapsulated drug (*W_en*). Thereafter, 30 mL of 5% sodium dodecyl sulfate (5%, v/w) was used to elute free PTX (*W_free*). The *EE*% [31] was calculated using the following formula:

$$EE\% = W_{en} / W_{total} \times 100\% \qquad (1)$$

In vitro drug release assay

In vitro drug release was measured by the dialysis method. Briefly, 1 mL of PTX-LMSNs solution was loaded into a prepreg dialysis bag (molecular weight cut-off = 8000-14000). The dialysis bag was then immersed in 20 mL of buffer containing 1% sodium dodecyl sulfate with pH = 5, 6.8 or 7.4 at a constant temperature of 37 °C while gently shaken at

100 r/min. A 2 mL aliquot of sample was withdrawn at 0, 1, 2, 4, 8, 12, 24, 48, 72, 96 and 120 h and subjected to HPLC analysis. The withdrawn sample was replaced with the same volume of fresh buffer. The experiment was repeated three times. The cumulative release rate (Q) of PTX was calculated using the following formula:

$$Q = (C_i V + \sum_{i=1}^{n-1} C_{i-1} \times 2)/M \times 100\% \quad (2)$$

where C_i is the sample concentration at the time point i, V is the volume of the suspension plus the release medium in the dialysis bag, and M is the dose of PTX in the dialysis bag.

In vivo biodistribution

Comply with the ARRIVE guidelines and were carried out in accordance with the U.K. Animals (Scientific Procedures) Act, 1986 and associated guidelines, and EU Directive 2010/63/EU for animal experiments. C57 Mice were depilated and anesthetized by intraperitoneal injection with 1.3 g/kg uratan solution (> 98%, 65mg/mL), and injected intravenously with 0.1 mL of fluorescent Rhodamine-LMSNs. The mice were imaged at 5, 30, 120 and 360 min post-injection and euthanized for 6 h after imaging. The heart, liver, spleen, lungs and kidneys were dissected, washed with deionized water and placed in a Petri dish. The tissues were imaged at an excitation wavelength of 550 nm and an emission wavelength of 600 nm for a fixed exposure time of 0.1 s. After the experiment, the mice were euthanized by cervical spondylolysis.

Pharmacokinetics analysis

Animal experiments have been approved by the Institutional Animal Care and Use Committee of Guangdong Pharmaceutical University and comply with the ARRIVE guidelines and were carried out in accordance with the U.K. Animals (Scientific Procedures) Act, 1986 and associated guidelines, and EU Directive 2010/63/EU for animal experiments. SD Rats were fasted and weighed 12 h before the experiment. The animals were randomly divided into two groups (6 per group, equal number of male and female) and injected with 20 mg/kg PTX-LMSNs via the tail vein. Blood samples (250 µL) were collected via the retroorbital route at 0, 0.083, 0.5, 1, 2, 3, 4, 6, 8 and 12 h post-injection and placed in heparin-coated tubes. After the experiment, rats were euthanized by inhaling CO_2. The blood samples were centrifuged at 3000 r/min for 10 min, and the upper plasma layer was collected. The plasma (100 µL) was mixed with an equal volume of acetonitrile, vortexed for 1 min, sonicated for 1 min (40 kHz, 300 W), and then centrifuged at 10000 r/min for 10 min. The samples were then analyzed by HPLC.

Statistical analysis

SPSS17.0 statistical software was used for statistical analysis. The data were expressed as mean ± standard deviation (SD). Comparison of the tested samples with the control samples was carried out by analysis of variance and t-test. $P < 0.05$ was considered statistically significant.

Results

Characterization of MSNs and PTX-LMSNs

MSNs were morphologically characterized by SEM and TEM. As shown in the SEM images in Figure 1a, the MSNs had a uniform and regular spherical structure. Furthermore, TEM analysis verified the presence of pores on the MSNs, as indicated by the contrasting dark pore wall and bright channel in the images shown in Figure 1b. The particle diameter is about 150 nm. In addition, the pore walls appeared distinct and were densely arranged. TEM examination of the PTX-LMSNs (Figure 1c) revealed that they were spherical particles with a uniformly thick surface lipid layer and a distinct core-shell layer structure.

As shown in Figure 2a, the average particle size of MSNs was 225.6 ± 9.44 nm, and their PDI was 0.097 ± 0.02. These numbers indicate that MSNs have high stability and uniform particle size distribution. Furthermore, MSNs had a negative charge, according to their Zeta potential (Figure 2b). PTX-LMSNs also had a uniform particle size distribution, as indicated by the single symmetrical peak (Figure 2c). The average particle size and PDI of PTX-LMSNs were 245.8 ± 3.26 nm and 0.102 ± 0.02, respectively. Although the particle size of MSNs increased as a result of lipid modification, it remained at around 220 nm. In addition, the lipid shell had no effect on PDI, indicating that the incorporation of phospholipids did not interfere with the stability of the MSNs. As shown in Figure 2d, the lipid modification also did not cause a significant change in Zeta potential, which remained in a range of -15 to -30 mV.

According to the IUPAC nomenclature, the adsorption of MSNs belongs to a typical type IV isotherm [32]. The pore size distribution of MSN was narrow, and the average pore size was about 3.05 ± 0.04 nm, which is a suitable size allow the incorporation of PTX.

Drug loading and encapsulation efficiency (EE) of PTX-LSNs

The DL and EE of PTX-LMSNs were 21.75 ±

4.28% and 96.36 ± 1.93%, respectively. This may be due to the fact that most drug molecules were loaded into the mesoporous silica pores, and only a few of them were adsorbed on the outer surface; these may cause a small amount of drug to dissociate into the solution during the preparation of lipid layer. The high drug loading and high encapsulation efficiency of PTX-LMSNs make them have significant clinical translational value, which can improve the therapeutic effect of paclitaxel and reduce the toxicity and side effects, providing a new strategy for the clinical application of tumor targeted therapy.
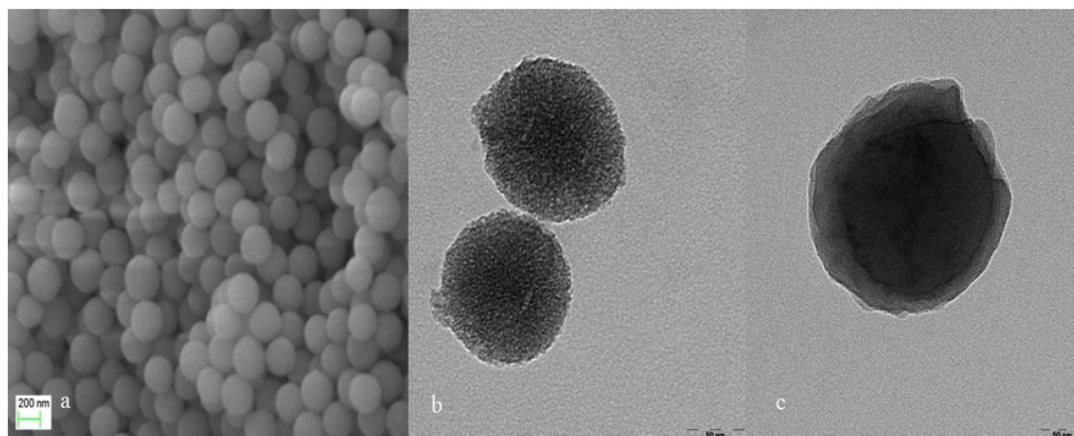

Figure 1. (a) SEM image of MSNs. (b) TEM image of PTX-MSNs. (c) TEM image of PTX-LMSNs.
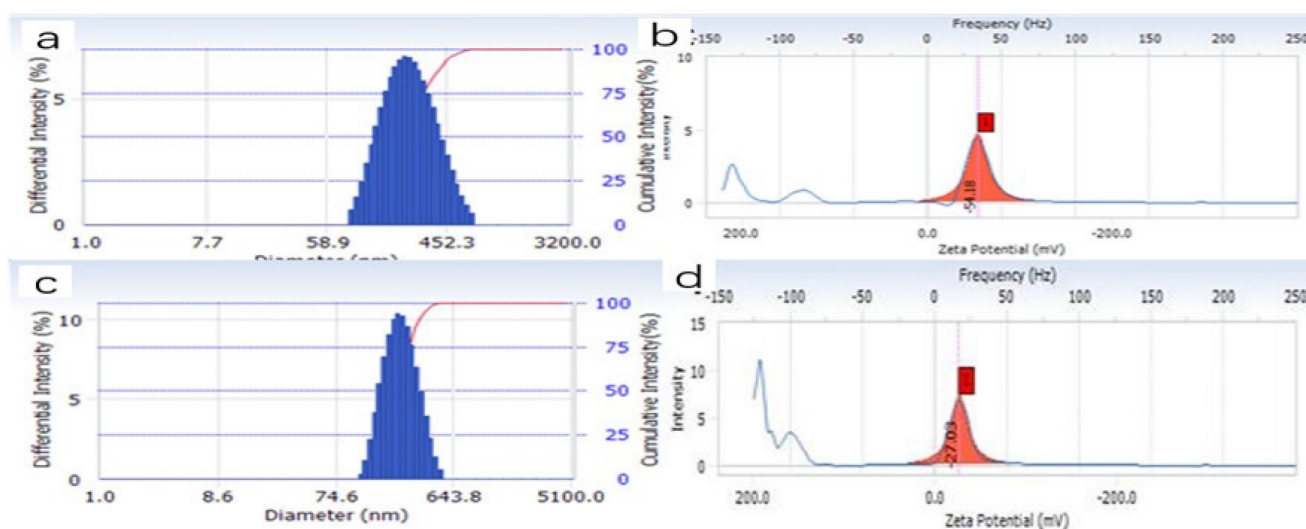

Figure 2. Particle size distribution and zeta potential of MSNs. (a) Particle size distribution of PTX-LMSNs. (b) Zeta potential of MSNs. (c) Particle size distribution of PTX-LMSNs. (d) Zeta potential of PTX-LMSNs.
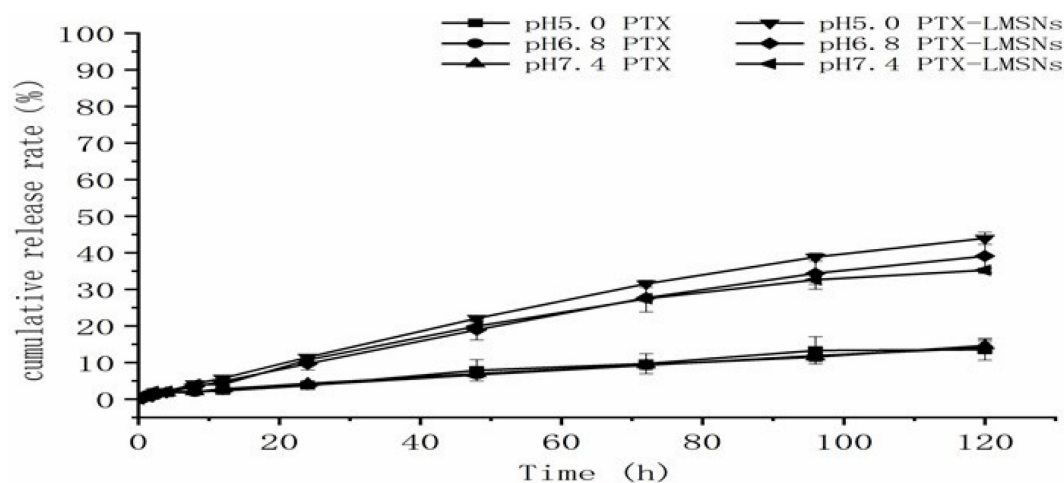

Figure 3. *In vitro* release profile of PTX from PTX-LMSNs under different pH conditions.

In vitro release of PTX from PTX-LMSNs

Unlike weakly alkaline healthy tissues, tumors have a low pH due to the Warburg effect wherein the increase of oxygen consumption leads to the production of acidic metabolites [33]. Therefore, we exposed PTX-MSNs and PTX-LMSNs to different pH levels that simulate the pH of normal tissues (pH 7.4), extracellular fluid of tumor tissues (pH 6.8) and the endosomes or lysosomes (pH 5), and then measured the amount of drug released at 37 °C. As shown in Figure 3, the cumulative amount of PTX released from the LMSNs was 3-4 times higher than that released from the unmodified MSNs at all tested pH conditions, which is an indication sustained drug release. Furthermore, the cumulative amount of drug released per unit time from PTX-LMSNs was highest at pH 5;11.48% of the encapsulated drug was released within 24 h, 22.07% within 48 h, and 43.98% within 5 days. This can be attributed to the instability of phospholipid membranes under acidic conditions [34]. Protons in an acidicc medium can accelerate the replacement of the drug, thus leading to its rapid release. Therefore, the LMSN carrier is pH-sensitive and can selectively release the drug cargo at the tumor site. The cumulative increase of PTX in the acidic tumor tissues can not only improve the efficacy of the drug but also minimize the damage to normal tissues and cells.

Biodistribution of antitumor drug in mice

Distribution and fluorescence intensity of PTX-LMSNs in mice are illustrated in Figure 4. The probe entered the body circulation within 5 min of injection, and the fluorescence intensity of PTX-LMSN in the abdomen increased with time and was especially high in the liver and spleen. In addition, the strong fluorescence in the bladder may be related to drug metabolism. The fluorescence intensity of PTX-LMSNs in the bladder decreased after 2 h of administration. After 6 h, fluorescence was nearly undetectable in any of the organs.

Organs were removed 6 h after administering with the PTX-LMSNs and subjected to *ex vivo* fluorescence imaging. As shown in Figure 5, the drug mainly accumulated in the liver, which could be due to the abundance of macrophages that can recognize opsins (serum proteins) adsorbed on the surface of the nanoparticles. Hepatic accumulation enhances the anti-tumor effect by increasing the local concentration of paclitaxel at the site of liver tumors while reducing systemic distribution to minimize side effects; however, excessive accumulation may increase the metabolic burden on the liver, leading to drug-induced liver injury or diminished efficacy against metastasis to other organs. Modifying dosage forms and using combination therapy strategies can maximize benefits and reduce risks.

The pharmacokinetic parameters of Taxol and the PTX-LMSNs were fitted by DAS software with the two-compartment model and are summarized in Table 2. As shown in Figure 6, the *in vivo* half-life of PTX-LMSNs was 23.21% higher than that of Taxol, and the area under the curve (AUC) was twice as high, an indication of longer drug retention, higher therapeutic efficacy and lower toxicity.

Table 2. Pharmacokinetic parameters in mice (n=5).

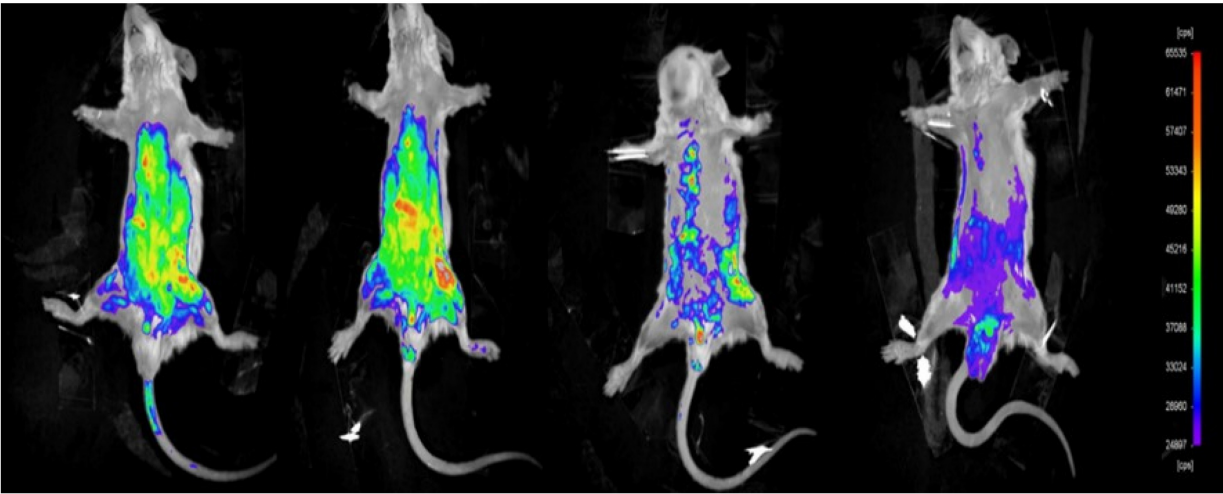| Parameters	Taxol	LMSNs
$t_{1/2\alpha}$/h	0.056	0.069
$t_{1/2\beta}$/h	1.208	0.287
Vd/L*Kg-1	234.833	155.146
K21/h-1	4.201	5.109
K10/h-1	1.476	3.241
K12/h-1	7.363	4.157
AUC/mg·L-1·h	28.848	51.707
CL/L·h-1·kg	346.642	502.835

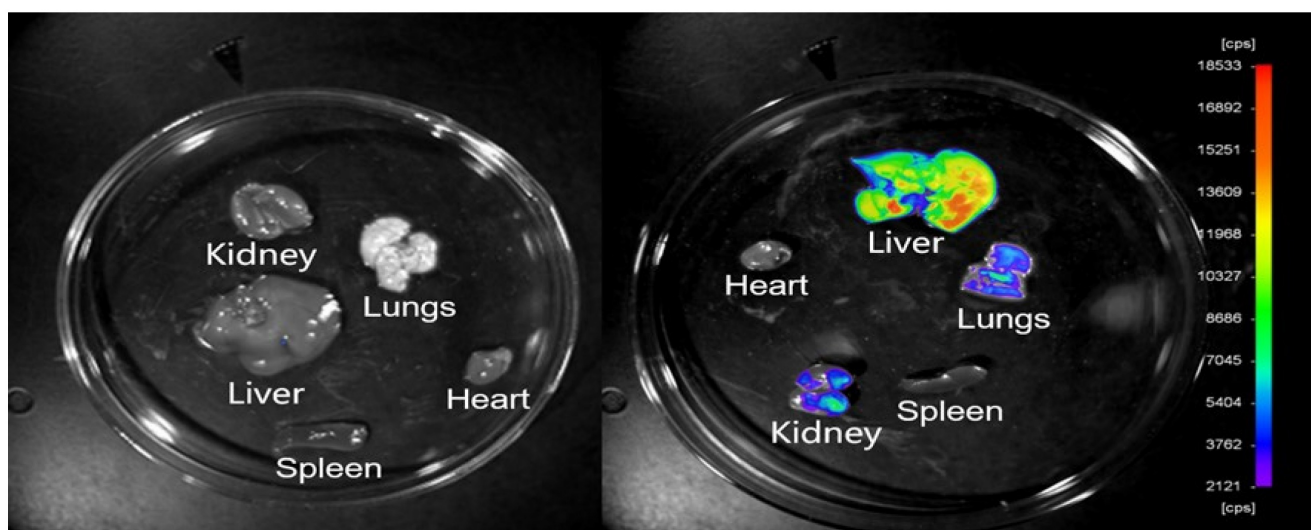**Figure 4.** Distribution and fluorescence intensity of PTX-LMSNs probe in mice.

Figure 5. Tissue distribution of fluorescent PTX-LMSN (a: control; b: PTX-LMSNs)
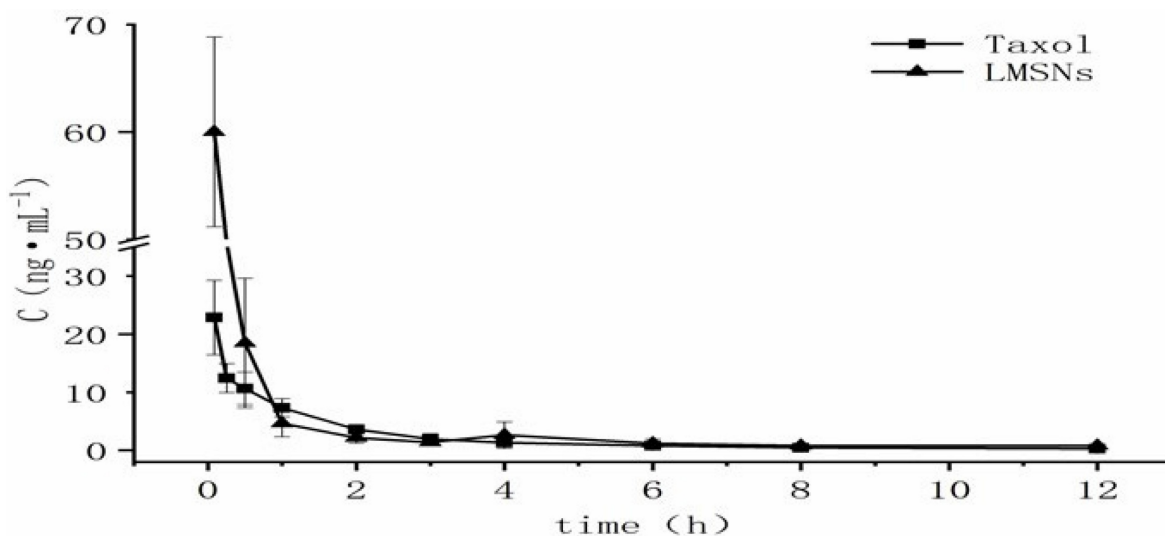

Figure 6. Concentration-time curve.

Conclusions

We successfully prepared PTX-LMSNs by fusing liposomes with MSNs. PTX-MSNs were sensitive to low pH, making them ideal drug carriers for the acidic TME, as they could be controlled to release the drug cargo in a pH-responsive manner. The targeted delivery of the drug cargo to the tumor site improves therapeutic efficacy while minimizing damage to normal tissues. Real-time *in vivo* near-infrared fluorescence imaging showed a fairly board large size distribution range of PTX-LMSNs, which may be related to their low metabolism. Visceral fluorescence intensity map further indicated that PTX-LMSNs were mainly clustered in the liver. This can be attributed to the fact that the abundant macrophages in the liver can recognize opsins (serum proteins) adsorbed on the surface of the nanoparticles. *In vivo*

pharmacokinetics showed that PTX-LMSNs had a higher AUC compared to that of Taxol, indicating that they have longer retention. This property is beneficial for high drug efficacy and low toxicity. PTX-LMSNs exhibit high drug loading, small particle size, and pH-responsive drug release, which have significant advantages in preclinical studies. Subsequently, it is necessary to promote its transformation into clinical trials through system toxicology evaluation, process scale-up and optimization, and targeting efficiency optimization. This study provides a new strategy for the development of nanocarrier-based tumor targeted delivery systems, but it is necessary to further address the issues of large-scale production and long-term safety.

Abbreviations

PTX: paclitaxel; MSNs: Mesoporous silica

nanoparticles; LMSNs: lipid-shell mesoporous silica nanoparticles; PTX-LMSNs: paclitaxel-loaded lipid-shell mesoporous silica nanoparticles; SEM: Scanning electron microscopy; TEM: Transmission electron microscopy; DL%: The Drug loading; EE%: Entrapment efficiency; HPLC: High performance liquid chromatography; TEOS: Ethyl orthosilicate; CTAB: Cetyltrimethyl ammonium bromide; Solutol: HS-15 15-hydroxy Stearic acid polyethylene glycol; PDI: Polydispersion index; BET: Brunauere-Emmette-Teller; BJH: Barrett-Joyner-Halenda; SD: Standard deviation; AUC: Area under the curve.

Acknowledgements

Availability of data and materials

All data supporting the conclusions of this article are included within the article.

Ethics approval and consent to participate

Animal experiments have been approved by the Institutional Animal Care and Use Committee of Guangdong Pharmaceutical University and comply with the ARRIVE guidelines and were carried out in accordance with the U.K. Animals (Scientific Procedures) Act, 1986 and associated guidelines, and EU Directive 2010/63/EU for animal experiments.

Author contributions

All authors listed above made substantial, direct, and intellectual contributions to the work discussed in this publication. Y.Z and HC.L. designed the article. Wang GQ, Xiao M, Ban JF, Deng YY, Zhou JR, Zhan T, Su ZH, Cao YS, Luo JX, Zhao LM and Hua JJ performed the experiments, analyzed the data, and drafted the paper. All authors discussed the data and revised the manuscript. All authors have read and agreed to the published version of the manuscript.

Competing Interests

The authors have declared that no competing interest exists.

References

1. Eknoyan G, Beck GJ, Cheung AK, et al. Effect of dialysis dose and membrane flux in maintenance hemodialysis. N Engl J Med. 2002; 347: 2010-9.
2. Yadav P, Ambudkar SV, Rajendra PN. Emerging nanotechnology-based therapeutics to combat multidrug-resistant cancer[J]. J Nanobiotechnology. 2022;**20**(1):423.
3. Anderski J, Mahlert L, Sun J, et al. Light-responsive nanoparticles based on new polycarbonate polymers as innovative drug delivery systems for photosensitizers in PDT[J]. Int J Pharm. 2019;**557**:182-191.
4. Kovtareva S, Kusepova L, Tazhkenova G, et al. Surface Modification of Mesoporous Silica Nanoparticles for Application in Targeted Delivery Systems of Antitumour Drugs[J]. Polymers (Basel). 2024;**16**(8).
5. Chen D, Liu X, Lu X, et al. Nanoparticle drug delivery systems for synergistic delivery of tumor therapy[J]. Front Pharmacol. 2023;**14**:1111991.
6. Hobson JJ, Al-Khouja A, Curley P, et al. Semi-solid prodrug nanoparticles for long-acting delivery of water-soluble antiretroviral drugs within combination HIV therapies[J]. Nat Commun. 2019;**10**(1):1413.
7. Sy P M, Anton N, Idoux-Gillet Y, et al. Pickering nano-emulsion as a nanocarrier for pH-triggered drug release[J]. Int J Pharm, 2018; **549**(1-2):299-305.
8. Vyas S P, Goswami R. Size-dependent cellular uptake and TLR4 attenuation by gold nanoparticles in lung adenocarcinoma cells[J]. Nanomedicine (Lond), 2019;**14**(3):229-253.
9. Cheng H, Liao J, Ma Y, et al. Advances in targeted therapy for tumor with nanocarriers: a review[J]. Mater Today Bio. 2025;**31**:101583.
10. Din F U, Aman W, Ullah I, et al. Effective use of nanocarriers as drug delivery systems for the treatment of selected tumors[J]. Int J Nanomedicine, 2017;**12**:7291-7309.
11. Sun H, Li X, Liu Q, et al. pH-responsive self-assembled nanoparticles for tumor-targeted drug delivery[J]. Journal of Drug Targeting, 2024;32(6): 672-706.
12. Wang B, Hu S, Teng Y, et al. Current advance of nanotechnology in diagnosis and treatment for malignant tumors[J]. Signal Transduct Target Ther. 2024;**9**(1):200.
13. Sun L, Liu H, Ye Y, et al. Smart nanoparticles for cancer therapy[J]. Signal Transduct Target Ther. 2023;**8**(1):418.
14. Tong R, Hemmati H D, Langer R, et al. Photoswitchable nanoparticles for triggered tissue penetration and drug delivery[J]. J Am Chem Soc. 2012;**134**(21):8848-8855.
15. Nam J, Won N, Jin H, et al. PH-Induced aggregation of gold nanoparticles for photothermal cancer therapy[J]. J Am Chem Soc. 2009;**131**(38):13639-13645.
16. Yu Y, Zhang X, Qiu L. The anti-tumor efficacy of curcumin when delivered by size/charge-changing multistage polymeric micelles based on amphiphilic poly(beta-amino ester) derivates[J]. Biomaterials. 2014;**35**(10):3467-3479.
17. Raza A, Rasheed T, Nabeel F, et al. Endogenous and Exogenous Stimuli-Responsive Drug Delivery Systems for Programmed Site-Specific Release[J]. Molecules. 2019;24(6):1117-1117.
18. Lee CH, Cheng SH, Wang YJ, et al. Near-Infrared Mesoporous Silica Nanoparticles for Optical Imaging: Characterization and *In Vivo* Biodistribution. Advanced Functional Materials. 2009;19: 215-222.
19. Watermann A, Brieger J. Mesoporous Silica Nanoparticles as Drug Delivery Vehicles in Cancer[J]. Nanomaterials (Basel). 2017;**7**(7).
20. Kankala R K, Liu C, Yang D, et al. Ultrasmall Platinum Nanoparticles Enable Deep Tumor Penetration and Synergistic Therapeutic Abilities through Free Radical Species-Assisted Catalysis to Combat Cancer Multidrug Resistance[J]. Chemical Engineering Journal. 2019;**383**:123138.
21. Kovtareva S Y, Kopishev E E, Zhang H, et al. Exploring the physicochemical interactions and loading strategies of mesoporous silicon dioxide nanoparticles for drug delivery[J]. Eur J Pharm Biopharm. 2025;**208**:114654.
22. Xu B, Li S, Shi R, et al. Multifunctional mesoporous silica nanoparticles for biomedical applications[J]. Signal Transduct Target Ther. 2023;**8**(1):435.
23. Kim S, Diab R, Joubert O, et al. Core-shell microcapsules of solid lipid nanoparticles and mesoporous silica for enhanced oral delivery of curcumin[J]. Colloids Surf B Biointerfaces, 2016;**140**:161-168.
24. Zhang B B, Chen X J, Fan X D, et al. Lipid/PAA-coated mesoporous silica nanoparticles for dual-pH-responsive codelivery of arsenic trioxide/paclitaxel against breast cancer cells[J]. Acta Pharmacol Sin. 2021;**42**(5):832-842.
25. Sun Y, Xu Y, Sun Y, et al. Synthetic methods of lipid-coated mesoporous silica nanoparticles as drug carriers[J]. Biointerphases. 2022;**17**(2):20801.
26. Sivadasan D, Sultan M H, Madkhali O, et al. Polymeric Lipid Hybrid Nanoparticles (PLNs) as Emerging Drug Delivery Platform-a Comprehensive Review of their Properties, Preparation, Methods, and Therapeutic Applications[J]. Pharmaceutics. 2021;**13**(8).
27. Biswas S, Kumari P, Lakhani P M, et al. Recent advances in polymeric micelles for anti-cancer drug delivery[J]. Eur J Pharm Sci. 2016;**83**:184-202.
28. Huang R, Shen Y W, Guan Y Y, et al. Mesoporous silica nanoparticles: facile surface functionalization and versatile biomedical applications in oncology[J]. Acta Biomater.2020;**116**:1-15.
29. Laranjeira M S, Ribeiro T P, Magalhaes A I, et al. Magnetic mesoporous silica nanoparticles as a theranostic approach for breast cancer: Loading and release of the poorly soluble drug exemestane[J]. Int J Pharm. 2022;**619**:121711.
30. Lin J, Cai Q, Tang Y, et al. PEGylated Lipid bilayer coated mesoporous silica nanoparticles for co-delivery of paclitaxel and curcumin: Design, characterization and its cytotoxic effect[J]. Int J Pharm. 2018;**536**(1):272-282.
31. Zhang X, Zhu Y, Fan L, et al. Delivery of curcumin by fucoidan-coated mesoporous silica nanoparticles: Fabrication, characterization, and *in vitro* release performance[J]. Int J Biol Macromol, 2022;**211**:368-379.

32. Esparza JM, Ojeda ML, et al. Development and sorption characterization of some model mesoporous and microporous silica adsorbents [J]. Journal of Molecular Catalysisi A: Chemical. 2005;228(1-2):97-110.

33. Rizzo R, Onesto V, Forciniti S, et al. A pH-sensor scaffold for mapping spatiotemporal gradients in three-dimensional in vitro tumour models[J]. Biosens Bioelectron, 2022;**212**:114401.

34. Moholkar D N, Sadalage P S, Havaldar D V, et al. Engineering the liposomal formulations from natural peanut phospholipids for pH and temperature sensitive release of folic acid, levodopa and camptothecin[J]. Mater Sci Eng C Mater Biol. 2021;**123**:111979.